Title: Dosage-dependent NF-κB oscillatory and heterogeneous dynamics in response to *E. Coli* Lipopolyssachride stimulation

Authors: Jaewook Joo[1], Jens Poschet[2], Catherine S. Branda[2], Bryan Carson[2], and Anup Singh[2]*

Affiliation: [1]Department of Physics, University of Tennessee, Knoxville, TN, 37996 USA; [2]Sandia National Laboratories, Livermore, CA & Albuquerque, NM, USA;

*Corresponding author email: aksingh@sandia.gov

Abstract: Cells sense external signal constantly, process it, and make its life-determining decision by using the embedded signal processing facilities. All of those events take place within an individual cell and thus should be studied at the level of single cells. Technical advances in live cell imaging make it possible to observe the time evolution of a protein abundance in single cells. Here we use a computational model, live cell fluorescence microscopy, and quantitative RT-PCR to investigate the translocation dynamics of a protein NF-κB and its biological relevance in single macrophages (RAW264.7 cells) when the cells are stimulated by *E. coli* lipopolysaccharide persistently. We incorporate into the computational model the signaling pathways of TLR4-MyD88-NF-κB, TNF-R and TNFα autocrine signaling and simulate heterogeneous NF-κB response in single cells, by taking into account the cell-to-cell variability in key protein copy numbers and kinetic rate constants. We present the fascinating yet puzzling NF-κB translocation dynamics as a response to different dosage of *E. coli* lipopolysaccharide: homogeneous oscillatory patterns of NF-κB for a large dosage and heterogeneous monotone-increasing patterns for a small dosage.

Key Words: live cell imaging; NF-κB protein dynamics; cell-to-cell variability; TNFα autocrine signaling; computational model; Oscillation

I. Introduction

A computational model, if corroborated with experimental data, can be transformed into a powerful analytic and predictive tool and can be used to guide the discovery processes in the biology research. Advancement in single live cell fluorescence microscopy makes possible to monitor the protein dynamics within single cells (Nelson *et al.* 2004; Lahav *et al.* 2004a; Geva-Zatorsky et al 2006). In this paper we investigated NF-κB dynamic response to persistent *E. coli* lipopolyssachride (LPS) stimulation of macrophages and especially its dependence on the dosage of stimulant, employing both computational model and live cell fluorescence microscopy. The current study provides a strong evidence of LPS-induced NF-κB oscillations, contradictory to the previous findings (Werner et al 2005; Covert et al 2005).

NF-κB is a stimulus-responsive pleiotropic regulator of gene control and plays significant roles on various parts of the immune system such as differentiation of immune cells, development of lymphoid organs, and immune activation (Verma and Stevenson 1997; Li and Verma 2002; Hoffmann and Baltimore 2006). NF-κB shuttling between nucleus and cytoplasm is directly related to the control of the expression of NF-κB target genes and thus bears physiological importance (Tian et al 2005). This shuttling is auto-regulated by the IKK- NF-κB-IκB-A20 signaling module, which consists of four proteins, inhibitor κB (IκB; there are at least three isoforms of it), IκB kinase (IKK), A20, and NF-κB. In the absence of external stimulus, IκB forms a protein complex with NF-κB, preventing NF-κB from entering into the nucleus. Stimulation induces the nucleo-localization of NF-κB: IKK is phosphorylated, phosphorylated IKK catalyses the ubiquitin-assisted degradation of IκB from the IκB: NF-κB complex, and, as a result, NF-κB is freed up to shuttle into the nucleus, initiating transcription of NF-κB target genes such as inflammatory cytokines (TNFα , IL-1, IL-6), chemokines (MIP-1α), anti-apoptotic (IAPs), and lastly but most importantly NF-κB signal termination (IκB isoforms and A20). NF-κB signal terminating proteins (IκB isoforms and A20) form

time-delayed negative feedback loops which enables NF-κB to readily oscillate between nucleus and cytoplasm (Tyson et al 2003).

TNFα stimulation induces a damped oscillatory NF-κB translocation pattern in a population of wild type embryonic mouse fibroblast cells (Hoffmann et al 2002). When IκBβ/IκBε double mutant cells are stimulated by TNFα, NF-κB dynamics averaged over millions of cells is highly oscillatory. However, in double mutants of IκBα/IκBβ knockouts, IκBα/IκBε knockouts, or in A20 single mutant cells, the average NF-κB dynamics over the millions of cells is non-oscillatory (or single-peaked). On the contrary to those population level experimental results, Nelson et al reported that NF-κB translocation dynamics are quasi-oscillatory and lasts for about 12 hours after TNFα stimulation, their using the live cell fluorescence imaging where fluorescence reporters of RelA and IκBα proteins are constructed into the wild type human AS-SK cells (Nelson et al 2004).

Covert et al in ref. (Covert et al. 2005) showed that the average NF-κB dynamics over a population of the E. coli LPS-insulted murine macrophages takes a non-oscillatory pattern (or a monotone increasing pattern). They conjectured that the source of this stable NF-κB response is a time difference between two signals reaching IKK: one signal comes directly from TLR4-MyD88-dependent signaling pathway and another comes indirectly from TLR4-TRIF-IRF3 pathway that activates TNF-R signaling pathway through newly synthesized TNFα after a time-delay. Werner et al in ref. (Werner et al 2005) presented the comparative study between the TNFα-stimulated NF-κB dynamics and the LPS-stimulated NF-κB dynamics: For TNFα stimulation, both IKK and NF-κB abundance levels peaks immediately after stimulation and quickly decrease. For LPS stimulation, however, the levels of IKK and NF-κB abundance slowly increase and reach their peaks about two hours after stimulation. They also conjectured that LPS-induced NF-κB dynamics is due to the TNFα autocrine signaling. Bosisio et al in ref. (Bosisio et al 2006) monitored NF-κB-bound IκBα promoter activity. The promoter activity upon TNFα stimulation shows a strong first pulse followed by very weak subsequent pulses:

i.e., TNF-R pathway is quickly inactivated right after TNFα stimulation. However, the promoter activity upon LPS stimulation demonstrates the first pulse followed by the stronger second pulse: TLR4 pathway activation is maintained for a prolonged duration for the case of LPS stimulation. All the previous studies agree that LPS stimulation may maintain prolonged pathway activation and induce a rising NF-κB profile, conjecturing that TNFα autocrine signaling may contribute to this characteristic of LPS stimulated NF-κB response.

Based upon accumulated knowledge of NF-κB signaling, Hoffmann *et al* built up a complex biochemical network model of IKK-NF-κB-IκB signaling (Hoffmann et al., 2002). This model was corroborated with their experimental data to demonstrate the functional roles of three isoforms of IκB: IκBα is responsible for sustained oscillatory translocation of NF-κB between cytoplasm and nucleus while IκBβ and IκBε make the NF-κB dynamics more damped (Hoffmann et al., 2002). Lipniacki et al adds a negative regulator of A20 to the previous model of Hoffmann et al with an assumption that A20 inactivates NF-κB signaling by inhibiting IKK phosphorylation (Lee et al 2000; Lipniacki et al., 2004). Hoffmann's group later on modified their model in various minor manners, but all of the variants share the same core components with the original model (Werner et al 2005; Kearns et al 2006; Krishna et al 2006; Cheong et al 2006). The above modeling efforts have been mainly focused on the deterministic methods. Hayot and Jayaprakash and others used a stochastic model of NF-κB signaling network to investigate the effect of both intrinsic and extrinsic noise on NF-κB translocation dynamics (Lipniacki et al 2006; Hayot and Jayaprakash 2006). They showed that averaging over many realizations of the stochastic NF-κB signaling system could unravel the discrepancy between oscillatory behaviors at single cells and damped-oscillation at a population of the cells. They also partially studied the effect of extrinsic noise (by the way of kinetic parameter variations) on protein dynamics. One of the authors investigated the intrinsic noise-induced oscillation of NF-κB and demonstrated its robustness against fluctuations in kinetic parameters (Joo et al 2010a and 2010b).

As shown in Fig. 1 and discussed in details in methods section, we make a novel comprehensive computational model of NF-κB signaling network consisting of the negative regulators of A20 and three isoforms of IκB. Moreover, we add TNFα autocrine signaling components to this comprehensive NF-κB network and investigate the effect of TNFα autocrine signaling, i.e., (+) feedback loop, on NF-κB dynamics. (+) feedback loops are prevalent in biology. (+) feedback loop in EGFR pathway induces bistability (or hysteresis) and a combination of (+) and (-) feedback loops brings about relaxation oscillation (Tyson et al 2003). In a system equipped with both (+) and (-) feedback loops, (+) feedback provides the (-) feedback loop-generated oscillation with tunable period and robustness (Tsai et al 2008).

As TNFα-stimulated NF-κB response differs dramatically between at a population of the cells (Hoffmann et al 2002) and at the single cells (Nelson et al 2004), LPS-stimulated NF-κB response at the level of single cells is expected to be quite different from the previously reported data at a population of the cells (Covert el al 2005; Werner et al 2005; Bosisio et al 2006). Thus, the previous conjectures about the effect of (+) feedback loop on the NF-κB dynamics needs to be validated both experimentally and theoretically at the level of single cells. In addition, this effect on NF-κB dynamics is expected to depend on the dosage of stimulant.

In this paper, we study NF-κB translocation dynamics in single macrophages (RAW264.7 cells) as a response to two different dosages (1 nM and 100 nM) of E. Coli Lipopolyssachride (LPS), taking into account the effect of TNFα autocrine signaling on the NF-κB response. To make the computational model specific to LPS stimulation and inclusive of TNFα autocrine signaling, we incorporate into the computational model the signaling pathways of TLR4-MyD88-NF-κB, TNF-R, and TNFα autocrine signaling (a positive feedback loop). In addition, our computational model is designed to simulate heterogeneous NF-κB response in single cells, by taking into account the extrinsic noise-driven cell-to-cell variability. We predict and explain the dosage-dependent characteristics of NF-κB translocation dynamics at single cells by using the

computational model, and corroborate and verify them by live cell fluorescence imaging experiments. First, using the computational model alone, we present that the TNFα autocrine signaling induces the bistability, resulting in two equilibrium levels of nuclear NF-κB and extracellular TNFα in a broad range of the parameter values in the TNF-R signaling pathway. The low equilibrium level of nuclear NF-κB is four orders of magnitude times smaller than the high level. Assuming that the signaling system can have either one of two equilibrium levels of nuclear NF-κB before LPS stimulation, we demonstrate that only the system with the low level of nuclear NF-κB exhibits noticeable NF-κB response to the low (1 nM) dosage stimulation and the system with the high level is not responsive at all. For the high (100 nM) dosage stimulation, however, the system with either high or low level of nuclear NF-κB induces a similar dynamical response. Second, both the experiments and the computations show that the LPS stimulation induces three heterogeneous dynamic patterns of NF-κB translocation (single-peaked, damped oscillatory, and rising patterns) and their distribution is dosage-dependent. The high dosage (100 nM) stimulation induces more homogeneous dynamic patterns than the low dosage (1 nM). Third, both experiments and computations reveal that, for the high (100 nM) dosage stimulation, both the majority and their population average of the nuclear NF-κB profiles at the level of single cells are highly (under-damped) oscillatory, which is in contrast to the previous findings of Covert et al 2005. On the contrary, the low (1 nM) dosage stimulation induces non-oscillatory dynamics (a rising pattern) of NF-κB in the population average and almost a half of the cells. Fourth, by using only the computational model, we validate the conjecture: the TNFα autocrine signaling is responsible for a rising pattern of NF-κB. When stimulated by the low dosage (1nM), the TNFα knocked-out computational model doesn't give rise to the rising pattern. Lastly, we use the real time quantitative PCR of A20 mRNA and IκBα mRNA to demonstrate the correlation between the dosage-dependent NF-κB translocation dynamics and the expression profiles of NF-κB target genes.

II. Results

To unravel the underlying mechanisms of how the low and the high LPS dosages induce different dynamic response of NF-κB at the level of single cells, we employ the computer model to generate testable predictions of the characteristics of NF-κB dynamic response and verify them by single cell fluorescence imaging.

Computational model for LPS-induced NF-κB dynamic response and TNF autocrine signaling: One of the NF-κB target genes is TNFα. A newly synthesized TNFα followed by NF-κB nuclear localization is released extracellularly and activates TNFα pathway. This results in the activation of canonical NF-κB signaling pathway and thus forms (+) feedback loop. A minimally required set of the activated pathways to model LPS-stimulated NF-κB dynamics should include TLR4-MyD88 dependent pathway, canonical NF-κB pathway, TNFα autocrine pathway, and TNF-R pathway. The computational model network (detailed in method section) consists of TNFα autocrine signaling (positive feedback loop) as well as (-) feedback loops by A20 and IκB isoforms. The NF-κB dynamics on this network is determined by the interplay between (+) and (-) feedback loops. The NF-κB in the delayed (-) feedback loop oscillates in a restricted parameter space (Krishna et al 2006; Joo et al 2010a) and It is expected that TNFα (+) feedback loop can make this oscillation amplified and robust (Tyson et al 2003).

TNFα autocrine signaling, (+) feedback loop, gives rise to the bistability of NFKB response. For the analysis of the bistability, we consider only the TNF-R, canonical NF-κB, and TNFα autocrine signaling pathways as shown in Fig. 1A. For the simplicity of our analysis, we suppose that NF-κB nuclear localization leads to the mRNA and protein synthesis of TNFα followed by the export of intracellular TNFα proteins without any additional regulatory mechanisms. In the absence of external stimulus, nuclear NF-κB level will ever increase if there exists only a (+) feedback loop. But, because our model system composes of both (+) and (-) feedback loops, their interplay stabilizes the system. Moreover, (+) feedback loop introduces its well-known

characteristics into the (-) feedback loop controlled system: bistability and amplification of the (-) feedback-driven behavior such as oscillation. To demonstrate the existence of the bistability in our model system, we choose one of the kinetic reactions in TNF-R pathway, the activation of IKK by IKKKa as shown in Fig. 1A, and vary its rate to simulate the varying strength of (+) feedback loop. Both steady state levels of extracellular TNFα and nuclear NF-κB depend on the strength of (+) feedback loop. In fact, the extracellular level of TNFα is inter-related with the nuclear level of NF-κB because the nuclear NF-κB regulates the synthesis of TNFα. As presented in Supporting Fig. 1, as the strength of (+) feedback increases, both stationary levels of extracellular TNFα and nuclear NF-κB discontinuously jump from a low to a high value sharply at a strength of (+) feedback. Likewise, as this strength decreases, both steady state responses discontinuously drop down from a high to a low value at the lower strength of (+) feedback. This discontinuity is a signature of the bistability, but the bistable range of (+) feedback strength is too small to be recognizable in Supporting Fig. 1. Moreover, the levels of nuclear NF-κB and TNFα remains almost invariant across the four orders of magnitude of the change in (+) feedback loop strength except at the discontinuity: For a weak (+) feedback, the equilibrium level of nuclear NF-κB is in order of 0.001 nM while it is in order of 10 nM for a strong (+) feedback. This leads us to conjecture that the canonical NF-κB signaling system supplemented/amplified by TNFα autocrine signaling can have either low or high equilibrium level of nuclear NF-κB and its response to external stimulus can be dramatically different, depending on which strength of (+) feedback the signaling system possesses, or in the other words, which equilibrium level of nuclear NF-κB the system has before the stimulation. This possibility is computationally explored and presented at a later section, but remains subject to future experimental validation.

Extrinsic noise drives cell-to-cell variability and heterogeneous NF-κB response in single cells: We use a statistical ensemble analysis to simulate the extrinsic noise and its effect on NF-κB dynamics in the single cells (Joo et al 2010b). Briefly stated, extrinsic noise is modeled as fluctuations in the network parameters such as the copy number of key proteins and kinetic rate constants. A population of the single cells is

represented by an ensemble of 1000 replicates of the signaling system and the network parameters of individual replicate are sampled from the uniform distribution defined uniquely by both the reference values of the kinetic rate constants and the universal interval size χ. For this paper, the heterogeneity measure is set to χ=30%. This statistical ensemble analysis generates heterogeneous NF-κB dynamics collected from the ensemble of 1000 replicate systems as shown in Fig. 2.

Distribution of NF-κB heterogeneous dynamic patterns depends on LPS dosage: Each NF-κB temporal profile is different from one replicate to anther. Individual NF-κB profiles, however, can be simply classified into one of four dynamic patterns: under-damped oscillation, sustained oscillation, single-peaked pattern, or hyperbolic pattern. We stimulate the ensemble of the signaling system with two different stimulant strengths, classify the resulting profiles of NF-κB dynamics, and measure the percent of the profiles belonging to the class of a dynamic pattern for each dosage. High dosage stimulation (LPS=100 nM) leads to a skew distribution of the dynamic patterns: a majority of the nuclear NF-κB profiles are oscillatory patterns. But, low dosage stimulation (LPS=1 nM) induces the evenly distributed dynamic patterns and the more heterogeneous distribution of the dynamic patterns. Thus, extrinsic noise drives cell-to-cell variability in NF-κB response and high dosage stimulation suppresses this variability

As discussed in method section, we tag the RelA protein with green fluorescent protein (GFP) and monitor the RelA translocation patterns in the single cells in real time for four hours after LPS stimulation. The time-varying nuclear GFP intensity per cell is quantified and normalized by the maximum nuclear GFP intensity from a single movie shot. (We present only nuclear GFP intensity because the cytoplasmic GFP intensity remains relatively non-dynamical and invariant.) We take at least two to three movie replicates for each dosage and confirm that for the same dosage stimulation, the GFP-RelA dynamics is consistent between replicates. In Fig. 3A and 3B, about 40 individual time-series are presented for each of two different E. Coli LPS dosage stimulations, 1 nM and 100 nM. Each curve represents the normalized nuclear GFP-RelA intensity in an individual cell. We take the average nuclear GFP-RelA intensity over those 40 cells

captured in the field of microscopic observation. This average corresponds to a population level behavior, though the number of the cells is quite small compared to the millions of the cells in typical experimental measurements.

Small LPS dosage induces more heterogeneous NF-κB response than large dosage: We calculate the standard deviation of nuclear GFP-RelA temporal profiles away from their average for low and high LPS dosage stimulations. The standard deviation decreases in time for low LPS dosage stimulation while it increases for high LPS dosage stimulation as shown in the top panels in Fig. 3A and 3B. In addition, each individual curve is classified into one of three dynamic patterns: under-damped oscillation, rising pattern, and single-peaked pattern. This classification shows that the distribution of the dynamic patterns of GFP-RelA protein is dependent on the LPS dosage. Low dosage induces evenly distributed dynamic patterns while when stimulated by high LPS dosage, about 75% of cells exhibit a single dynamic pattern, damped-oscillatory response. So we experimentally verify the model prediction that low dosage induces more heterogeneous response in single cells than high dosage does. The above observation can be quantified by entropy measure, defined as $H=-\sum_i P_i \log P_i$ where P_i is a fraction of *i*th dynamic pattern, which is a good indicator of heterogeneity of the dynamic patterns. The entropy amounts to $H=0.33$ for high dosage and $H=0.46$ for low dosage. The higher entropy for lower dosage indicates that the dynamic patterns are more disordered and heterogeneous for lower dosage stimulation.

Large LPS dosage induces oscillatory NF-κB response: The computational model assumes that the LPS stimulation activates first TLR4-MyD88 dependent pathway and subsequently the (+) feedback loop consisting of canonical NF-κB signaling, TNFα autocrine signaling, and TNF-R signaling pathway. Before the LPS stimulation, the signaling system can reach either one of two equilibrium levels of nuclear NF-κB, a low level for a weak (+) feedback and a high level for a strong (+) feedback. We find that, upon high dosage stimulation (LPS=100 nM) to TLR4-MyD88 dependent pathway, both weak and strong (+) feedback strengths induce the similar NF-κB response. As shown in

Fig. 3A, high dosage stimulation (LPS=100 nM) induces a highly (under-damped) oscillatory pattern in both a majority of the ensemble and their ensemble average regardless of the strength of (+) feedback. In other words, the ensemble consisting of the copy systems with different (+) feedback strengths and the resulting equilibrium levels of nuclear NF-κB exhibits the fairly homogenous distribution of the NF-κB dynamic response, which shoots up in less than one hour, followed by the subsequent pulses with decreasing peak amplitudes. The underlying mechanism of the high dosage-stimulated NF-κB behavior indifferent of (+) feedback strength is rather simple. The high dosage stimulation (LPS=100 nM) is strong enough to override whatever may be the pre-existing condition of the ensemble. The system with the high equilibrium level of nuclear NF-κB, i.e., the one with strong (+) feedback, also have the high level of negative regulators of A20 and IκB isoforms, which readily suppresses the nuclear translocation of NF-κB. On the one hand, if we were to observe the noticeable dynamic response of NF-κB, the signal strength should be high enough to override the pre-existing strong negative regulation. On the other hand, we can expect that the sufficiently low dosage stimulation can induce quite a different NF-κB response in the ensemble of the systems with weak (+) feedback strength than that with strong (+) feedback strength.

Low LPS dosage induces a rising pattern of nuclear NF-κB: Upon low dosage stimulation (LPS=1 nM), the ensemble with strong (+) feedback strength exhibits totally different NF-κB dynamic response from the ensemble with weak (+) feedback strength. As shown in Fig. 2, the former ensemble barely exhibits any noticeable change in nuclear NF-κB level while the latter ensemble shows the substantial increase of nuclear NF-κB level. In contrast to the oscillatory NF-κB response from high dosage stimulation, the low dosage induces a non-oscillatory rising pattern of nuclear NF-κB but only in the ensemble with weak (+) feedback strength. Both the majority of the individual profiles and their average show this rising pattern: The second peak of nuclear NF-κB profile is as high as the first peak and the subsequent peaks increase in time until the nuclear NF-κB level reaches its equilibrium level determined by the interplay of (-) and (+) feedbacks.

The rising pattern of nuclear NF-κB follows the rising profile of extracellular TNFα in Fig. 2B.

We demonstrate that the underlying mechanism of this low dosage-induced rising pattern originates from TNFα autocrine signaling. To prove our assertion, we employ a standard biology technique of knocking out TNFα and comparing two NF-κB profiles, one from the wild type and another from the mutant. When TNFα is knocked out, the rising trend of nuclear NF-κB evidently present in the wild type disappears at once as shown in Fig. 2B. This *in silico* knocked-out experiment partially confirms the undeniable effect of TNFα (+) feedback loop on the rising pattern of nuclear NF-κB upon low dosage stimulation.

As shown in Fig. 3A, upon high (100 nM) E. Coli LPS dosage stimulation, the majority of GFP-RelA profiles and their average take an under-damped oscillatory pattern. The most common characteristic of the individual GFP-RelA responses is the strong first peak followed by the weak second peak. As expected, the individual profiles of nuclear GFP-RelA in the single cells are not at all similar to the monotone-increasing nuclear NF-κB profile at the population level reported in ref. (Covert et al 2005). On the contrary, the low (1 nM) E. Coli LPS dosage stimulation induces a rising response of nuclear NF-κB in both a majority of GFP-RelA profiles and their average as shown in Fig. 3B. A characteristic of this rising pattern is the increasing peak amplitude of GFP-RelA: the large second peak follows the small first peak.

Nuclear NF-κB dynamics and mRNA profiles of IκBα and A20 are correlated: We investigate the relationship between the NF-κB dynamic response and the expression of NF-κB target genes. For this purpose, we use quantitative RT-PCR to measure the induction level of IκBα mRNA, A20 mRNA, and RelA mRNA at multiple time points with and without stimulation with two different LPS dosages. The mRNA profiles are presented in Fig. 3A for 100 nM E. Coli LPS and in Fig. 3B for 1 nM E.Coli LPS. Without stimulation, the induction levels of all three mRNAs remain close to the level of house keeping genes with small fluctuations. In regard to the dynamic pattern, mRNA profiles show LPS-dosage independent behavior. For both 1 nM and 100 nM LPS

stimulations, two distinctive peaks are observed at the time points of 45 and 120 minutes, for both A20 mRNA and IκBα mRNA and the second peak is substantially smaller than the first peak. Upon high LPS dosage stimulation, the mRNA profiles (not shown here) are nicely correlated with the NF-κB response in Fig. 2A. The timing of the first and the second peaks of the mRNA profiles of A20 and IκBα correspond to the peaks of the nuclear NF-κB, taking into consideration of about half an hour delay for mRNA synthesis. But, for low LPS dosage stimulation, the rising pattern of nuclear NF-κB in Fig. 2B is not correlated with the mRNA profiles in Fig. 3: the source of the second peak of mRNA profile cannot be identified from the rising pattern of nuclear NF-κB profile whose second peak occurs one hour after the occurrence of the second peak of mRNA. But, the maximum induction level of A20 and IκBα depends on the LPS dosage. The first peak amplitudes of A20 and IκBα mRNA profiles are substantially higher for the larger LPS dosage (data not shown). In addition, RelA mRNA induction level is hardly changed throughout the course of stimulation except some fluctuations (data not shown). This invariant RelA level confirms our assumption of a conservation of total NF-κB copy number.

III. Discussion

We demonstrate that the NF-κB protein dynamics in the identical cells under the same environmental conditions take not a uniform dynamic pattern, but a few well-defined heterogeneous dynamic patterns. This non-uniform cellular behavior among the individual cells cannot be easily derived from the population level measurements, and dramatically different from the previous assumptions about the biological dynamics, i.e., its robustness and uniformity. Two points that are worth to mention are the source of this cell-to-cell variability in protein dynamics and its physiological consequence. Regarding the source, it remains still open what can derive this large cell-to-cell variability. Intrinsic noise, defined as randomness of the collisions between biochemical species, alone cannot explain this heterogeneity because the observed dynamic patterns are much more heterogeneous than what intrinsic noise can generate (Hayot and Jayaprakash 2006; Joo et al 2010b). The other source is termed as extrinsic noise that originates from the outside

of the signaling system through the coupling of the system with the fluctuating environmental conditions and other noisy signaling and/or regulatory modules. Extrinsic noise affects all genes simultaneously and can be modeled as fluctuations in kinetic rate constants that influence fluctuations in the copy number of key proteins. Assuming that this extrinsic noise can certainly generate heterogeneous protein dynamics (Paulsson 2004; Joo et al 2010a and 2010b), we proposed a novel statistical ensemble analysis to deal with the extrinsic noise-driven heterogeneity in ref. (Joo et al 2010b). In this paper, we validate our proposal by demonstrating that computationally simulated extrinsic noise can reproduce the experimentally observed heterogeneous dynamics of NF-κB. Concerning physiological effect of extrinsic noise, this cell-to-cell variability in protein dynamics significantly affects the cell-fate decision and can be a prominent source of drug resistance. For example, Alon's group exhibited the heterogeneous dynamics of a few proteins that are related to drug resistance (Cohen et al 2008). Because NF-κB plays an important role in not only so many biological functions such as apoptosis, inflammation, immune cell differentiation but also cancer angiogenesis and chemotherapy, the observed large cell-to-cell variability in NF-κB translocation dynamics should significantly affect the normal and the abnormal cellular functions. This connection needs to be investigated in the future.

Some of our results at the single cell level are in contrast to the previous observations at the population level (Covert et al 2005; Werner et al 2005). The difference between ours and the previous studies arises from two sources: (1) the noise-driven dynamics in the single cells and (2) the LPS dosage. Both Covert et al and Werner et al reported that, when the single murine macrophages are stimulated by LPS, the nuclear NF-κB profile averaged over a population of the cells takes a monotone increasing pattern. They used two low LPS dosages, 0.1 μg/ml (0.2 nM) and with 0.5 μg/ml (1 nM). Consequently, their nuclear NF-κB profile resembles the rising pattern of nuclear NF-κB profile, a characteristic dynamic profile of LPS 1 nM stimulation, as shown in Fig. 3B. Based on the high LPS dosage stimulation data from the single cells, homogeneous and oscillatory NF-κB dynamics, we speculate that the nuclear NF-κB

profiles averaged over a population of the cells will show oscillatory behavior when stimulated by high enough LPS dosage.

Our studies indicate that the dosage of stimulant plays a significant role in the activation of inflammatory response and/or cell apoptosis. We show that stimulant dosage is correlated with the nucleo-cytoplasmic shuttling dynamics of a transcriptional protein NF-κB, which is in turn related with its target gene expression profile. It has been taken granted that dosage has a threshold behavior, i.e., response can occur only if the dosage is above the threshold value. But, in our paper, we relate low/high LPS dosage not with on/off response, but with different protein dynamics. We emphasize that each pattern of protein dynamics must have message/information.

We admit that our computational analysis is impartial and incomplete. The network is complex, large, and consists of many unknown parameters. Most of our conclusions are drawn from numerical simulations of the network only in a very restricted parameter space. It also lacks the understanding of the potential dynamics that this network can give rise to. One possible solution to overcome this shortcoming is to reduce the complexity of the model and analyze the dynamics in the reduced network. The network shown in Fig. 1A can be reduced to a simple network motif consisting of both (+) and (-) feedback loops: IκBα inhibits nuclear NF-κB, nuclear NFKB inhibits IκBα through TNFα autocrine signaling, NF-κB activates mRNA IκBα which in turn activates protein IκBα. This regulatory motif is equivalent to the "incoherently amplified negative feedback loop" (Tyson et al 2003). This delayed (-) feedback loop is known to oscillate in its own right and (+) feedback loop makes the oscillation amplified, robust, and tunable. (Tsai et al 2008). In addition to those already known mechanisms, it is desirable to investigate (1) how its dynamics (or oscillatory behavior) depends on the LPS dosage at the different strength of (+) and (-) feedback loops, (2) how its dynamics depends on the time-delay imposed on (+) and (-) feedback loops, (3) the effect of both intrinsic and extrinsic noise on the NF-κB dynamics in this reduced network, and (4) how extracellular TNFα contributes to homogenization and/or synchronization of the NF-κB dynamics at a population of the single cells.

IV. Methods

1. Computational network model: Our computational model consists of three modules, one for the canonical NF-κB signaling pathway shown in Fig. 1B, one for the TNF-R signaling pathway as shown in Fig. 1A, and one for the Toll like receptor 4 (TLR4-MyD88-dependent) signaling pathway as shown in Fig. 1A. The TNF-R and TLR4 signaling pathways converge on IKK, which initiates the canonical NF-κB signaling pathway. *E. Coli* LPS stimulates TLR4-MyD88-dependent signaling pathway. The signal propagates through this pathway and activates the canonical NF-κB pathway. Activated NF-κB translocates into the nucleus and initiates the transcription of NF-κB target genes. The newly synthesized TNFα stimulates TNF-R signaling pathway and the NF-κB signaling pathway, forming a positive feedback loop. Both A20 and IκB isoforms are negative regulators and form multiple negative feedback loops.

TNF receptor signaling pathway: As shown in Fig. 2A, TNF receptors (TNFR) become activated to be TNFR*, when bound by extracellular TNFα proteins. TNFR* can be reversed to TNFR when unbound. Activated TNF receptors (TNFR*) transform inactive IKK kinase into activated IKK kinase (IKKKa), which in turn activates neutral IκB kinase (IKKn) into activated IKK (IKKa). This initiates the canonical NF-κB signaling. This model was used by Lipniacki *et al* in their stochastic model (Lipniacki et al 2006).

TLR4-MyD88-dependent pathway: As shown in Fig. 2A, activation and inactivation of TLR4 occurs when LPS is bound or unbound to the receptors, respectively. Once LPS is bound to TLR4, the signal passes through a linear chain of the MyD88-dependent pathway and TAK can induce the activation of IKK (IKKa), activating the canonical NF-κB signaling pathway. The linear chain model of TLR4 signaling pathway was first used in ref (Selvarajoo 2006). This linear chain of multiple proteins is greatly simplified to a single super node by Covert et al. The only difference here is that we impose the conservation of the TLR4 mass in time: the sum of TLR4 and TLR4* should equal to a constant.

Canonical NF-κB signaling pathway (IKK-NF-κB-IκB-A20 signaling pathway): The NF-κB signaling pathway shown in Fig. 2B represents a new comprehensive model, i.e., the up-to-dated network comprising IκB kinase (IKK), NF-κB, both negative regulators of A20 and IκB isoforms (IκBα, IκBβ, IκBε), and the protein complexes formed by two or three of the constituents (Hoffmann et al., 2002; Lipniacki et al., 2004; Nelson et al., 2004; Lipniacki et al., 2006; Cheong et al., 2006; Covert et al., 2005; Kearns et al., 2006; Werner et al., 2005). This signaling pathway model also includes mRNA and protein syntheses of A20 and IκB isoforms. The network consists of 70 kinetic rate constants and one initial concentration of NF-κB, whose values are taken from the literature (Lipniaki et al 2004; Werner et al., 2005).

TNFα autocrine signaling: As shown in Fig. 2A, TNFα-mediated autocrine signaling is modeled as follows: the synthesis rate of mRNA TNFα (TNFt) depends on a saturating function of [NF-κBn] just as A20 mRNA and IKB mRNA do. TNFt is then translated to intracellular TNFα protein (TNFi). TNFi diffuses to extracellular space, becoming extracellular TNFα (TNFe), which is bound to TNF-R, making it activated TNF-R*.

Parameterization of the computational model with experimental data: The nominal values of most of the kinetic rate constants of the canonical NF-κB signaling pathway are taken from the literature (Lipniaki et al 2004; Werner et al., 2005). The synthesis rates and the degradation rates of A20 mRNA and IκBα mRNA are calibrated to reproduce the induction levels of the Q-PCR generated A20 mRNA and IκBα mRNA. The most significantly correlated parameter with NF-κB translocation dynamics is total NF-κB concentration and its value is taken from the literature. The volume ratio of cytoplasm to nucleus is the second most significantly correlated parameter with NF-κB response and its average and variation are measured from ten RAW 264.7 murine macrophage-like cells by Hyper-spectral imaging technique. Other available experimental data, e.g., both the IKK temporal profiles and the IκBα promoter-bound NF-κB profiles resulting from stimulation by either TNFα or LPS, are used as the qualitative patterns that our

computational model results should reproduce (Werner et al 2005; Covert et al 2005; Bosisio et al 2006).

Numerical simulation of the computational network model: The network in Fig. 2A is translated to a system of ordinary differential equations (ODE). These equations are simulated with the initial values of total NF-κB concentration and zero concentrations of all the other biochemical species. We simulate the ODE system until it reaches its equilibrium (33 hours) and then constantly stimulate the system and measure/record the temporal profiles of various biochemical species.

2. EGFP-RelA reporter construct: The $p_{\beta Actin}$-EGFP-RelA construct was derived from pECFP-F-RelA, a kind gift from Dr. Allan Brasier (University of Texas Medical Branch). ECFP was replaced with EGFP between the Age1 and BsrG1 sites, and the cytomegalovirus (CMV) promoter was replaced with a minimal 106bp human βActin promoter (1) cloned between the Ase1 and Nhe1 sites to reduce average expression levels. The plasmid pBA-GFP-RelA was linearized and used to transfect RAW264.7 murine macrophage-like cells (ATCC) by Nucleofection (Amaxa Biosystems). Transfected cells were grown for 12 days in the presence of G418, and a clone stably expressing GFP-RelA was isolated and named RG16.

3. RNA isolation and Quantitative RT-PCR: Total RNA is isolated from either RAW264.7 or RG16 murine macrophages stimulated with 0nM, 1nM or 100nM *E.coli* LPS at the following timepoints: 0, 30, 45, 60, 90, 120, 180, and 240min. The total RNA isolation is repeated on subsequent days to obtain two biological replicas for each experimental condition. Total RNA extraction is performed using Qiashredder, RNAeasy, and DNase on-column kits from Qiagen. RNA integrity is tested using a Bioanalyzer. Relative abundances of A20 and IκBα mRNA are measured using TaqMan® qRT-PCR with 50ng RNA per reaction. Probes, primers, and one step reagents are purchased from ABI and reactions are run in triplicate using an ABI 7500 instrument. Abundances are calculated relative to eukaryotic 18S rRNA using SDS v1.3 software (ABI).

4. Cell Culture, Transfection, and Imaging: RAW 264.7 cells are grown in DMEM supplemented with 10% fetal bovine serum, 2mM L-glutamine, 1mM sodium pyruvate, 1x MEM nonessential amino acids, 20mM HEPES, 100 I.U./ml penicillin, and 100μg/ml streptomycin. For microscopy, $3x10^5$ cells are plated in 35mm glass coverslip bottom dishes 18-24 hours prior to stimulation and imaging. Dishes are placed in a microscope stage-top humidified microincubator at 37°C with continuous flow 5% CO_2 in air. Stimulation is initiated by addition of growth medium containing lipopolysaccharide. Images are collected every 2-10 minutes for 4-6 hours.

V. Reference

[1] Nelson DE, Ihekwaba AEC, Elliott M, Johnson JR, Gibney CA, Foreman BE, Nelson G, See V, Horton CA, Spiller DG, Edwards SW, McDowell HP, Unitt JF, Sullivan E, Grimley R, Benson N, Broomhead D, Kell DB, White MRH (2004) Oscillations in NF-κB signaling control the dynamics of gene expression. Science 306: 704-708.

[2] Lahav G, Rosenfeld N, Sigal A, Geva-Zatorsky N, Levine AJ, Elowitz MB, Alon U (2004a) Dynamics of the p53-Mdm2 feedback loop in individual cells. Nat. Genet. 36: 147-150.

[3] Geva-Zatorsky N, Rosenfeld N, Itzkovitz S, Milo R, Sigal A. Dekel E, Yarnitzky T, Liron Y, Polak P, Lahav G, Alon U (2006) Oscillations and variability in the p53 system. Molecular Systems Biology.

[4] Werner SL, Barken D, Hoffmann A (2005) Stimulus specificity of gene expression programs determined by temporal control of IKK activity. Science 309: 1857-1861.

[5] Covert MW, Leung TH, Gaston JE, Baltimore D (2005) Achieving stability of lipopolysaccharide-induced NF-κB activation. Science 309: 1854-1857.

[6] Verma IM, Stevenson J (1997) IκB kinase: beginning, not the end. Proc Natl Acad Sci U S A 94: 11758-11760.

[7] Li Q, Verma, IM (2002) NF-κB regulation in the immune system. Nat. Rev. Immunol. 2: 725.

[8] Hoffmann A, Baltimore D (2006) Circuitry of nuclear factor κB signaling. Immunological Reviews 210: 171-186.

[9] Tian B, Nowak DE, Brasier AR (2005) A TNF-induced gene expression program under oscillatory NF-κB control. BMC Genomics 6: 137-155.
[10] Tyson JJ, Chen KC, Novak B (2003) Sniffers, buzzers, toggles ad blinkers: dynamics of regulatory and signaling pathways in the cell. Curr Opinion 15: 221-231.
[11] Hoffmann A, Levchenko A, Scott ML, Baltimore D (2002) The IκB-NF-κB signaling module: temporal control and selective gene activation. Science 298: 1241-1245.
[12] Bosisio D, Marazzi I, Agresti A,Shimizu N, Bianchi M E, and Natoli G (2006). A hyper-dynamic equilibrium between promoter-bound and ncleoplasmic dimmers controls NF-kB-dependent gene activity. EMBO Journal 25: 798-810.
[13] Lee EG, Boone DL, Chai S, Libby SL, Chien M, Lodolce JP, Ma A. (2000) Failure to regulate TNF-induced NF-κB and cell death responses in A20-deficient mice. Science 289: 2350-2354.
[14] Lipniacki T, Paszek P, Brasier AR, Luxon BA, Kimmel M (2004) Mathematical model of NF-κB regulatory module. J Theor Biol 228: 195-215.
[15] Kearns JD, Basak S, Werner SL, Huang CS, Hoffmann A (2006) IκBε provides negative feedback to control NF-κB oscillations, signaling dynamics, and inflammatory gene expression. J. Chem. Biol. 173: 659-664.
[16] Cheong R, Bergmann A, Werner S, Regal J, Hoffmann A, Levchenko A (2006) Transient IκB kinase activity mediates temporal NF-κB dynamics in response to a wide range of tumor necrosis factor-α doses. J. Biol. Chem. 281: 2945-2950.
[17] Krishna S, Jensen MH, Sneppen K (2006) Minimal model of spiky oscillations in NF-κB signaling. Proc. Natl. Acad. Sci. U S A 103: 10840-10845.
[18] Lipniacki T, Paszek P, Brasier AR, Luxon BA, Kimmel M (2006) Stochastic regulation in early immune response. Biophys J 90: 725-742.
[19] Hayot F, Jayaprakash C (2006) NF-κB oscillations and cell-to-cell variability. J. Theor. Biol. 240: 583-591.
[20] Joo J, Plimpton S, Faulon, JL (2010a). Noise-induced oscillatory shuttling of NF-κB in a two compartment IKK-NF-κB-IκB-A20 signaling model. ArXiv.org e-print is available at http://arxiv.org/abs/1010.0888.

[21] Joo J, Plimpton S, Faulon, JL (2010b). Novel statistical ensemble analysis for simulating heterogeneous response in NF-kB signaling network. ArXiv.org e-print is available at http://arxiv.org/abs/1010.0904.
[22] Tsai TY, Choi YS, Ma W, Pomerening JR, Tang C, Ferrell JE Jr. (2008) "Robust, tunable biological oscillations from interlinked positive and negative feedback loops" Science 321: 126-9.
[23] Paulsson J (2004) Summing up the noise in gene networks. Nature 427: 415-418.
[24] A. A. Cohen, N. Geva-Zatorsky, E. Eden, M. Frenkel-Morgenstern, I. Issaeva, A. Sigal, Ron Milo, C. Cohen-Saidon, Y. Liron, Z. Kam, L. Cohen, T. Danon, N. Perzov, U. Alon (2008). Dynamic Proteomics of Individual Cancer Cells in Response to a Drug Science 322: 1511.
[25] Selvarajoo K (2006) Discovering differential activation machinery of tehe Toll-like receptor 4 signaling pathways in MyD88 knockouts. FEBS Lett 580: 1457-64.
[26] Carlotti F, Chapman R, Dower SW, and Qwarnstorm EE (1999) Activation of nuclear factor *κB* in single living cells. J. Biolol. Chem. 274: 37941-37949.
[27] Liew FY, Xu D, Brint EK, O'Neil AJ (2005) Negative regulation of toll-like receptor-mediated immune responses. Nat. Rev. Immunol. 5: 446-458.
[28] Quitschke, W. W., Z. Y. Lin, et al. (1989). "The beta actin promoter. High levels of transcription depend upon a CCAAT binding factor." J Biol Chem **264**(16): 9539-46.

Figure Caption:

Figure 1: Extended network model of TNF-R, canonical NF-kappaB, and TLR4-MyD88 dependent signaling pathway. In (A) the activation of TLR4-MyD88-dependent pathway by LPS leads to the activation of a canonical NF-kappaB signaling pathway, which in turn activates the TNF-R pathway through TNF autocrine signaling. (B) shows IKK-IkappaB-NF-kappaB-A20 signaling pathway model.

Figure 2: Nuclear GFP-RelA amplitude from Live Single cell fluorescence microscopy data and computational model prediction. (A) includes about 40 individual profiles of GFP-RelA amplitude for 4 hours of experimental duration with persistent stimulation of 100 nM LPS. Different colored lines indicate GFP-RelA amplitudes from different cells. Thick red line represents the average profile and black dashed line denotes the standard deviation of individual curves from their average. (B) is for persistent stimulation of 1 nM LPS. In (C), the individual GFP-RelA profiles are classified into three clusters: single-peaked pattern for top panel, rising pattern for mid panel, and damped oscillatory pattern for bottom panel. The number in each panel indicates the percentage of the particular pattern and such a distribution of three patterns are presented in a bar graph in (D): blue for single-peaked pattern, orange for rising pattern and red for damped oscillatory pattern. In (E) and (F) are presented the classification and the distribution of the GFP-RelA profiles. Lastly, computational model prediction of the temporal profiles of the nuclear NF-κB concentration and its distribution are in (G) and (H) for 100 nM and in (I) and (J) for 1 nM persistent stimulation, respectively: yellow for sustained oscillatory pattern, red for damped oscillatory pattern and blue for single-peaked pattern.

Figure 3: Relative abundances of mRNA RELA and mRNA NF-κB target genes, IκBα and A20. mRNA levels of RELA in (A) and (D), IκBα in (B) and (E) and A20 in (C) and (F) are measured through quantitative PCR without (black lines) and with E. Coli LPS stimulation (red lines). Upper panels (A through C) are with 1 nM E. Coli LPS stimulation while the lower panels (D through F) are with 100 nM E. Coli LPS.

Supporting Figure 1: TNFα (+) feedback loops induces bistability and two equilibrium levels of nuclear NF-kappaB.

Supporting Figure 2: computer model prediction about the role of TNFα autocrine signaling on a rising pattern of nuclear NF-κB concentration upon 1 nM LPS stimulation. The blue curves are the nuclear NF-κB profiles from the ensemble of the NF-κB signaling network. A red curve represents the ensemble average of nuclear NF-κB profiles from a wild type case and a green curve denotes the ensemble average from a mutant with TNFα knocked-out.

Table I. Biochemical reactions & associated reaction rates in our computational model of the NF-κB signaling network. Column *I* is the kinetic parameter, *II* is its units, *III* is its nominal value from the reference, *IV* is the reference, and V is our nominal value. The reaction rates labeled with [1] are from Ref. [39], those labeled [2] are from Ref. [45], those labeled [3] use an average value between those in Ref. [39] & Ref. [45], those labeled [4] are from Ref. [Salvarjoo FEBS Lett], and those labeled from [5] are from Ref. [Cho et al]. The units for [a] are $\mu M^{-1}s^{-1}$, for [b] are s^{-1}, for [c] are $\mu M\ s^{-1}$, and for [d] are μM.

Reactions	I	II	III	IV	V
IKKa + IκBa → IKKa_IκBα	Aα	[a]	0.2	[1]	0.1813
IKKa + IκBb → IKKa_IκBβ	Aβ	[a]	0.05	[3]	0.02997
IKKa + IκBe → IKKa_IκBε	Aε	[a]	0.05	[3]	0.04244
IKKa+IkBα-NF-κB → IKKa-IκBα-NF-κB	Bα	[a]	1	[1]	1.024
IKKa+IkBβ-NF-κB → IKKa-IκBβ-NF-κB	Bβ	[a]	0.25	[3]	0.3683
IKKa+IkBε-NF-κB → IKKa-IκBε_NFkB	Bε	[a]	0.25	[3]	0.42
NF-κBn → NF-κBn + A20t	C1	[b]	0.0000005	[1]	0.000000506
0 → A20t	C2	[c]	0	[1]	0
A20t → 0	C3	[b]	0.0004	[1]	0.0002438
A20t → A20t + A20	C4	[b]	0.5	[1]	0.5807
A20 → 0	C5	[b]	0.0003	[1]	0.0003769
IKKa-IκBα → IKKa + IκBα	Dα	[b]	0.00125	[2]	0.002046
IKKa-IκBβ → IKKa + IκBβ	Dβ	[b]	0.00175	[2]	0.0005609
IKKa-IκBε → IKKa + IκBε	Dε	[b]	0.00175	[2]	0.002142
IKKa-IκBα-NF-κB → IKKa + IκBα-NF-κB	Dα	[b]	0.00125	[2]	0.002046
IKKa-IkBβ-NF-κB → IKKa + IκBβ-NF-κB	Dβ	[b]	0.00175	[2]	0.000561
IKKa-IκBε-NF-κB → IKKa + IκBε-NF-κB	Dε	[b]	0.00175	[2]	0.002142
IKKa-IκBα-NF-κB → IKKa-IκBα + NF-κB	Eα	[b]	0.000001	[2]	0.00000144
IKKa-IκBβ-NF-κB → IKKa-IκBβ + NF-κB	Eβ	[b]	0.000001	[2]	0.00000124
IKKa-IκBε-NF-κB → IKKa-IκBε + NF-κB	Eε	[b]	0.000001	[2]	0.00000064
IKKa-IκBα + NF-κB → IKKa-IκBα-NF-κB	Fα	[a]	0.5	[2]	0.3789
IKKa-IκBβ + NF-κB → IKKa-IκBβ-NF-κB	Fβ	[a]	0.5	[2]	0.2135
IKKa-IκBε + NF-κB → IKKa-IκBε-NF-κB	Fε	[a]	0.5	[2]	0.3528
IκBα-NF-κB → NF-κB + IκBα	Gα	[b]	0.000001	[2]	0.00000064
IκBβ-NF-κB → NF-κB + IκBβ	Gβ	[b]	0.000001	[2]	0.00000044
IκBε-NF-κB → NF-κB + IκBε	Gε	[b]	0.000001	[2]	0.00000069
IκBαn-NF-κBn → NF-κBn + IκBαn	Gα	[b]	0.000001	[2]	0.00000064
IκBβn-NF-κBn → NF-κBn + IκBβn	Gβ	[b]	0.000001	[2]	0.00000044
IκBεn-NF-κBn → NF-κBn + IκBεn	Gε	[b]	0.000001	[2]	0.00000069
IκBα + NF-κB → IκBα-NF-κB	Hα	[a]	0.5	[2]	0.4593
IκBβ + NF-κB → IκBβ-NF-κB	Hβ	[a]	0.5	[2]	0.7753

IκBε + NF-κB → IκBε-NF-κB	Hε	[a]	0.5	[2]	0.2895
IκBαn + NF-κBn → IκBαn-NF-κBn	Hα	[a]	0.5	[2]	0.4593
IκBβn + NF-κBn → IκBβn-NF-κBn	Hβ	[a]	0.5	[2]	0.7753
IκBεn + NF-κBn → IκBεn-NF-κBn	Hε	[a]	0.5	[2]	0.2895
NF-κB → NF-κBn	I1	[b]	0.0025	[1]	0.003037
NF-κBn → NF-κB	K01	[b]	0.00005	[3]	0.00005537
IKKn → IKKa	K1	[b]	0.0025	[1]	0.003273
A20 +IKKa → A20 + IKKi	K2	[a]	0.1	[1]	0.07075
IKKa → IKKi	K3	[b]	0.0015	[1]	0.00202
0 → IKKn	Kprod	[c]	0.000025	[1]	0.000009752
IKKn, IKKa, or IKKi → 0	Kdeg	[b]	0.000125	[1]	0.0001561
Volume ratio of cytoplasm to nucleus	Kv	1	5	[1]	Variable
IκBαn-NF-κBn → IκBα-NF-κB	Lα	[b]	0.01	[1]	0.013979
IκBβn-NF-κBn → IκBβ-NF-κB	Lβ	[b]	0.005	[3]	0.001567
IκBεn-NF-κBn → IκBε-NF-κB	Lε	[b]	0.005	[3]	0.006583
IκBα-NF-κB → NF-κB	Mα	[b]	0.000025	[1]	0.00002837
IκBβ-NF-κB → NF-κB	Mβ	[b]	0.000025	[3]	0.00003609
IκBε-NF-κB → NF-κB	Mε	[b]	0.000025	[3]	0.00000866
IKKa-IκBα-NF-κB → IKKa + NF-κB	Pα	[b]	0.1	[1]	0.12928
IKKa-IκBβ-NF-κB → IKKa + NF-κB	Pβ	[b]	0.05	[3]	0.06454
IKKa-IκBε-NF-κB → IKKa + NF-κB	Pε	[b]	0.05	[3]	0.08434
IκBαn → IκBα	Qα	[b]	0.0005	[1]	0.0005123
IκBβn → IκBβ	Qβ	[b]	0.0005	[3]	0.0007398
IkBεn → IkBε	Qε	[b]	0.0005	[3]	0.0002184
IKKa-IκBα → IKKa	Rα	[b]	0.1	[1]	0.123
IKKa-IκBβ → IKKa	Rβ	[b]	0.1	[3]	0.03837
IKKa-IκBε → IKKa	Rε	[b]	0.1	[3]	0.1571
IκBαn-NF-κBn → NF-κBn	Sα	[b]	0.000001	[2]	0.00000037
IκBβn-NF-κBn → NF-κBn	Sβ	[b]	0.000001	[2]	0.000001131
IκBεn-NF-κBn → NF-κBn	Sε	[b]	0.000001	[2]	0.000001037
NF-κBn → NF-κBn + IκBαt	Uα	[b]	0.0000005	[1]	0.000000279
NF-κBn → NF-κBn + IκBβt	Uβ	[b]	0	[2]	0
NF-κBn → NF-κBn + IκBεt	Uε	[b]	0.00000005	[3]	0.000000059
IκBα → IκBαn	Vα	[b]	0.001	[1]	0.0009786
IκBβ → IκBβn	Vβ	[b]	0.001	[3]	0.0004871
IkBε → IkBεn	Vε	[b]	0.001	[3]	0.00147
IκBα, IκBαn → 0	Wα	[b]	0.0001	[1]	0.000132
IκBβ, IκBβn → 0	Wβ	[b]	0.0001	[3]	0.000133
IκBε, IκBεn → 0	Wε	[b]	0.0001	[3]	0.000042
IκBαt → IkBαt + IkBα	Xα	[b]	0.5	[1]	0.4552
IκBβt → IκBαt + IκBβ	Xβ	[b]	0.5	[3]	0.3828
IκBεt → IκBαt + IκBε	Xε	[b]	0.5	[3]	0.3304
0 → IκBαt	Yα	[c]	0.00000005	[3]	0.000000084
0 → IκBβt	Yβ	[c]	0.000000005	[3]	0.00000000414
0 → IκBεt	Yε	[c]	0.000000005	[3]	0.00000000508

IκBαt → 0	Zα	[b]	0.0004	[1]	0.0003375
IκBβt → 0	Zβ	[b]	0.0004	[3]	0.0002031
IκBεt → 0	Zε	[b]	0.0004	[3]	0.0004742
Total NF-κB amount	$NF\kappa B_o$	[d]	0.06	[1]	Variable
LPS → MyD88	*Kf1*	[b]	0.1	[4]	0.1
MyD88 → 0	*Kb1*	[b]	0.1	[4]	0.01
MyD88 → IRAK	*Kf2*	[b]	0.1	[4]	0.1
IRAK → 0	*Kb2*	[b]	0.1	[4]	0.1
IRAK → TRAF	*Kf3*	[b]	0.1	[4]	0.1
TRAF → 0	*Kb3*	[b]	0.1	[4]	0.1
TRAF → TAK	*Kf4*	[b]	0.1	[4]	0.1
TAK → 0	*Kb4*	[b]	0.1	[4]	0.1
NF-κBn → NF-κBn + TNFt	*Qf1*	[b]	0.025	[5]	0.0000007
TNFt → 0	*Qb1*	[b]	0.025	[5]	0.0005
TNFt → TNFi	*Qf2*	[b]	0.025	[5]	0.5
TNFi → 0	*Qb2*	[b]	0.025	[5]	0.00005
TNFi → TNFe	*Qf3*	[b]	0.025	[5]	0.0003
TNFe → 0	*Qb3*	[b]	0.025	[5]	0.05
TNFe + TNFR → TNFR*	*Qf4*	[b]	0.025	[5]	0.1
TNFR* → TNFR	*Qb4*	[b]	0.025	[5]	0.01
TNFR* + IKKKn → IKKKa	*Qf5*	[b]	0.025	[5]	0.1
IKKKa → IKKKn	*Qb5*	[b]	0.025	[5]	0.01
IKKKa + IKKn →IKKa	*Qf6*	[b]	0.025	[5]	0.001

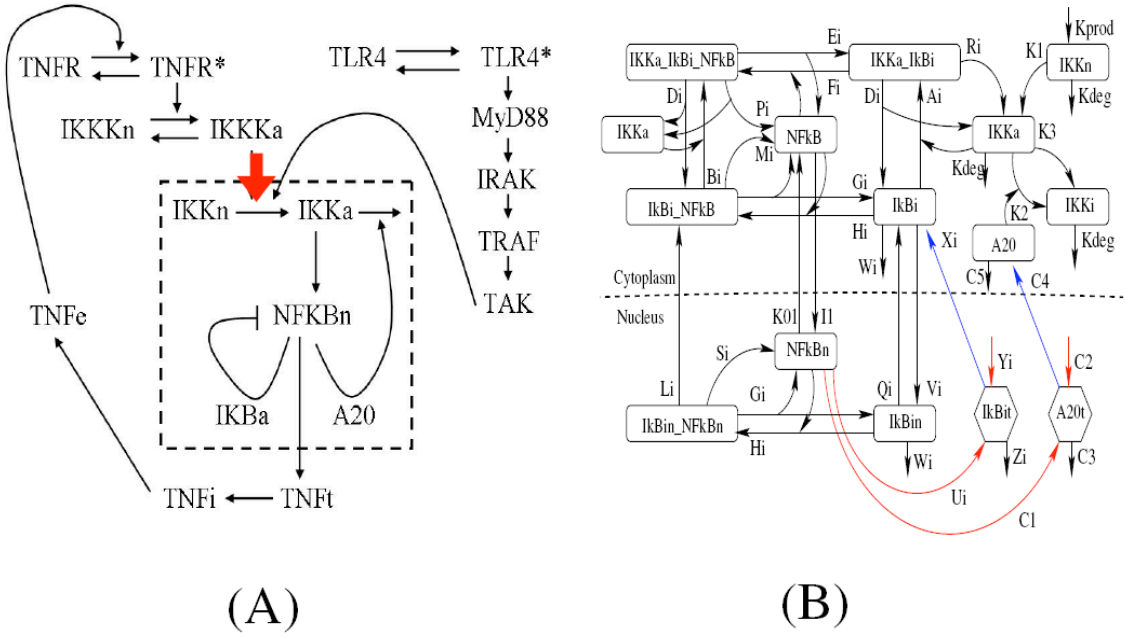
TNFR
TNFR*
IKKKn
IKKKa
TLR4
TLR4*
MyD88
IRAK
TRAF
TAK
IKKn
IKKa
NFKBn
IKBa
A20
TNFe
TNFi
TNFt
(A)
IKKa_IkBi_NFkB
IKKa_IkBi
IKKa
NFkB
IkBi_NFkB
IkBi
IKKn
IKKi
A20
Kprod
K1
K2
K3
Kdeg
Ei
Ri
Di
Fi
Ai
Pi
Mi
Bi
Gi
Hi
Wi
Xi
C5
C4
Cytoplasm
Nucleus
K01
I1
NFkBn
Si
Li
Qi
Vi
IkBin_NFkBn
IkBin
IkBit
A20t
Yi
C2
Zi
C3
Ui
C1
(B)

Figure 1

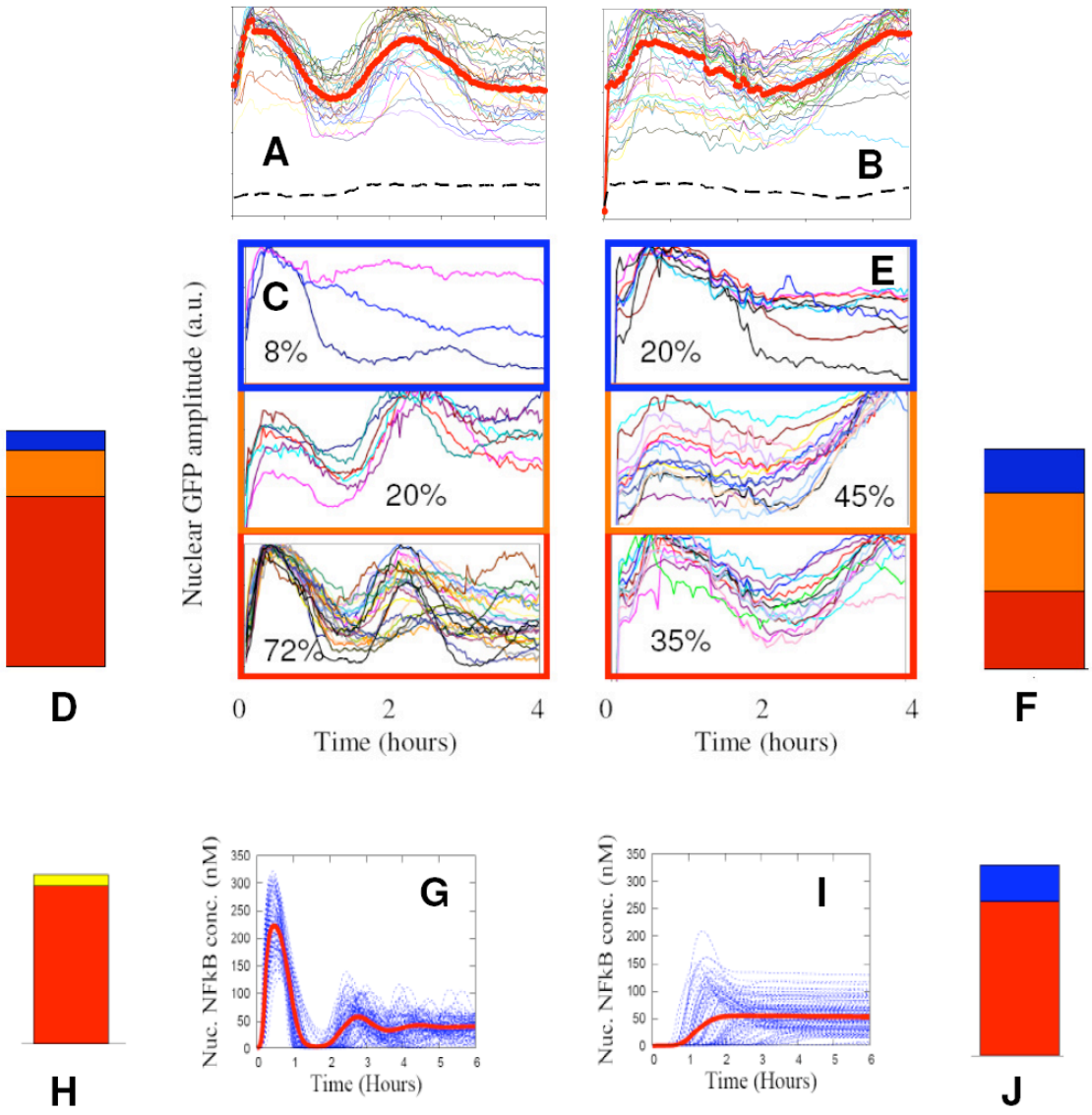
A
B
C
8%
20%
72%
E
20%
45%
35%
Nuclear GFP amplitude (a.u.)
0
2
4
Time (hours)
0
2
4
Time (hours)
D
F
H
J
G
Nuc. NFkB conc. (nM)
Time (Hours)
I
Nuc. NFkB conc. (nM)
Time (Hours)

Figure 2

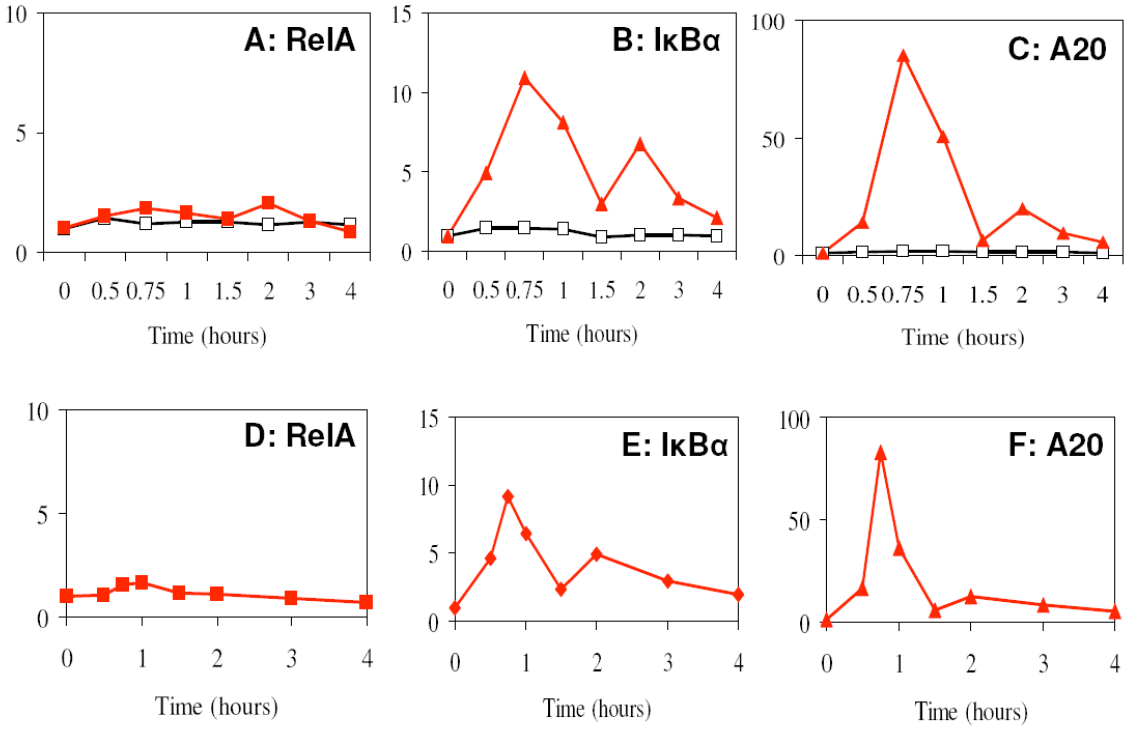
A: RelA
B: IκBα
C: A20
D: RelA
E: IκBα
F: A20
Time (hours)
Time (hours)
Time (hours)
Time (hours)
Time (hours)
Time (hours)

Figure 3

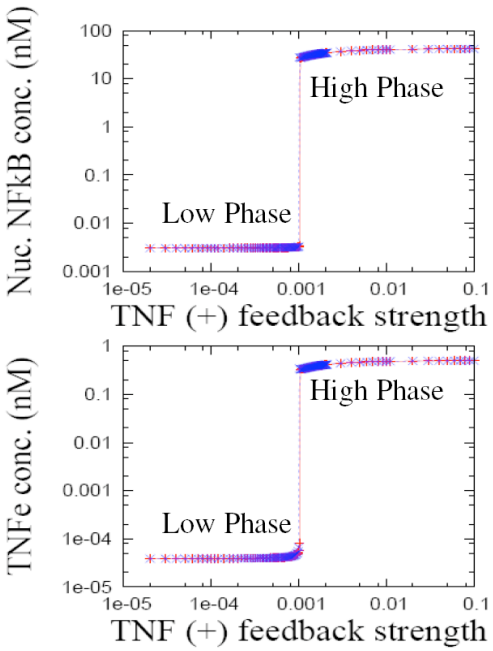

Supporting Figure. 1

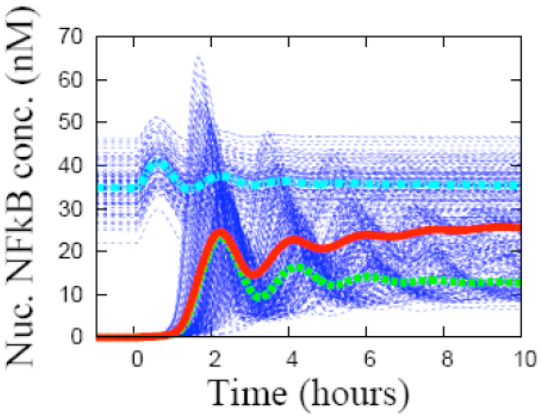

Supporting Figure 2.